Chemical Engineering Journal 498 (2024) 155496

Contents lists available at ScienceDirect

Chemical Engineering Journal

journal homepage: www.elsevier.com/locate/cej

Toxic metals removal by new membranes based on graphene oxide and a cationic Polymer: Influence of chemical and morphological aspects

Tauany de Figueiredo Neves [a,b], Cláudia Batista Lopes [b], Valmor Roberto Mastelaro [c], Renato Falcão Dantas [a], Carlos Manuel Silva [b,*], Patrícia Prediger [a,*]

[a] Limeira School of Technology, University of Campinas, PO Box 456, 13484-332 Limeira, S.P., Brazil
[b] CICECO - Aveiro Institute of Materials, Department of Chemistry, University of Aveiro, Campus Universitário de Santiago, 3810-193 Aveiro, Portugal
[c] São Carlos Institute of Physics, University of São Paulo, PO Box 369, 13566-590, São Carlos, S.P., Brazil

ARTICLE INFO

Keywords:
Polymeric nanocomposite membranes
Layer-by-layer assembly
Adsorption
Selective membranes
Multicomponent systems

ABSTRACT

Polymeric nanocomposite membranes are emerging as promising materials for water treatment. To explore the potential of new materials for the removal of toxic metals from water, novel hydrolyzed polyacrylonitrile (hPAN) membranes coated with graphene oxide (GO) by layer-by-layer (LbL) assembly, using poly(4-vinylpyridinium iodide) (PVPI) as binding agent, were prepared, characterized, and applied to remove toxic metals in multi-component systems. The addition of PVPI and GO to the hPAN membrane modified the surface roughness, hydrophilicity, layers morphology, and introduced oxygenated functions to the pristine polymer. These features enhanced the material's selectivity for Cu^{2+}, Cr^{3+}, and Pb^{2+}, over Ni^{2+} and Cd^{2+}, with removal efficiencies of 50.4 %, 64.3 %, and 99.9 % in batch assays, at the concentrations of 4.1, 12.2, and 10.2 mg L^{-1}, and selectivities relative to Cd^{2+} of 13.7, 24.2 and 13450, respectively. Governed by the formation of coordination complexes, the increment of nanocomposite layers adhered to the polymer improved the adsorbent/adsorbate interactions. The efficiency of hPAN membrane with three PVPI/GO bilayers in removing metal ions was attested in comparison to other polymer nanocomposite membranes from literature.

1. Introduction

Heavy metals are frequently classified as high-density metallic elements, being commonly used in mining, electroplating, and electronics manufacturing industries [1]. Additionally, they are usually incorporated into products such as paints, pesticides, light bulbs, fertilizers, and personal care products [2]. Some heavy metals can be toxic to humans and other organisms and can be released into the environment in combination with different classes of contaminants, such as complex dyes, organophosphates, and phenolic compounds. The most commonly detected metals in water bodies are cadmium (Cd), lead (Pb), copper (Cu), chromium (Cr), mercury (Hg), and nickel (Ni) [3]. Recently, Sankhla *et al.* [4] reported high concentrations of Ni and Pb ions in the Yamuna River in India. As one of the major tributaries of the Ganges River, the Yamuna River is the water source for several metropolitan cities in India, and according to the authors the average concentration of Pb^{2+} and Ni^{2+} in the river over a period of one year was 1.9–0.24 mg L^{-1} and 1.83–0.12 mg L^{-1}, respectively. These values are considerably higher than those recommended by the World Health Organization (WHO), which stipulates maximum concentrations of 0.001 and 0.002 mg L^{-1} for Pb^{2+} and Ni^{2+}, respectively [5].

With adverse effects for aquatic fauna and flora, and for humans, when present in relevant concentrations, toxic metals have been found with increasing frequency in water, wastewater, and effluents, mainly due to the widespread use and inefficiency of the conventional water treatments employed [6]. Efficient methods to remove such contaminants from dilute systems are adsorption and/or ion exchange (*i.e.*, sorption). These methods are based on the mass transfer of pollutants from solution to the solid phase where they accumulate onto the internal surface (adsorption) or replace stoichiometrically the solid counter ions. Adsorption is a mature and efficient technique with low implementation and maintenance costs. Since it relies on solid–fluid chemical and/or physical interactions, its efficiency depends on the adsorbent materials employed [7].

In recent years, nanotechnology-based products have been explored as potential adsorbent materials for the removal of toxic metals from

* Corresponding authors at: Limeira School of Technology, University of Campinas, PO BOX 456, 13484-332 Limeira, S.P., Brazil (P.Prediger). CICECO, Department of Chemistry, University of Aveiro, Campus Universitário de Santiago, 3810-193 Aveiro, Portugal.
E-mail addresses: carlos.manuel@ua.pt (C.M. Silva), prediger@unicamp.br (P. Prediger).

https://doi.org/10.1016/j.cej.2024.155496
Received 28 February 2024; Received in revised form 29 July 2024; Accepted 3 September 2024
Available online 5 September 2024

water. Nanomaterials have properties such as high specific surface area, good pore size distribution, and enhanced sites for adsorbent/adsorbate interactions [8]. A variety of potential nanoadsorbents has been used to remove toxic metals, including graphene derivatives, carbon nanotubes, and metal oxide-based nanoparticles. Despite the advantages of using nanomaterials for adsorption, a limiting factor is their high colloidal stability, which makes it difficult to remove them after the adsorption process. Thus, one of the alternatives to overcome this challenge is the immobilization of nanoadsorbents in polymeric structures [9].

Considered barriers with the ability to select the permeation of certain chemical species, membranes are emerging as a versatile strategy in the water purification process due to their cost-effectiveness, high efficiency, and low environmental impact [10]. From this perspective, the incorporation of nanoadsorbents in the polymeric matrix modifies the physical–chemical properties of the membrane, contributing to or interfering with its functionality. The trade-off between the enhancement of adsorbent properties of membranes and the formation of structural defects in the polymeric matrix that compromise the integrity of their structure depends on the manufacturing technique employed. Several techniques for preparing polymeric nanocomposite membranes have been explored, including physical deposition, electrospinning, phase inversion, and layer-by-layer (LbL) assembly [8].

With the objective to explore the preparation of new membranes with potential to remove toxic metals from water, and to understand how the incorporation of new nanoadsorbents in the polymeric matrix influences membrane efficiency, this study addresses the synthesis, characterization, and application of a new polymeric nanocomposite membrane for the removal of multiple toxic metals from water. New hydrolyzed polyacrylonitrile (hPAN) membranes coated with graphene oxide (GO) and poly(4-vinylpiridinium iodide) (PVPI) were prepared in this essay by LbL assembly, using PVPI as binding agent.

Endowed with nitrile groups with potential for partial hydrolysis, polyacrylonitrile (PAN) has electron-rich and electron-poor centers that enhance its interactions with metal ions [11]. Even so, due to their average pore size, which is slightly larger than the contaminant molecules, and the high flow rates usually encountered in practice, hPAN membrane are overlooked in favor of other polymers for water and effluent treatment. In this context, the use of GO in the hPAN membrane aims to improve the membrane permeation process. GO, a nanoadsorbent obtained by the incomplete oxidation of graphite and subsequent exfoliation, can chemically and physically influence membrane properties. In the chemical aspect, since GO has oxygen functional groups, it can enhance the formation of coordination complexes between such composite membranes and metal ions [12], and in the physical aspect GO alters membrane size and the distribution of pores, roughness, and hydrophilicity, parameters that influence the selectivity and anti-fouling [13] of the materials. However, because they have negative charges, GO and hPAN tend to repel each other electrostatically, requiring the presence of a cationic material as an electrostatic attracting agent between the two materials. In this case, we opted to use a cationic polymer (PVPI), which besides having bactericidal activity [14], would also provide the membrane with cation-π attraction, enhancing adsorbent/adsorbate interactions [15]. The choice for heavy metal contaminants was due to their different atomic radii, which made it possible to study the adsorption selectivity towards metals according to the number of GO/PVPI layers on the membrane.

The new membranes, denominated hPAN/PVPI/GO, were characterized by Fourier transform infrared spectroscopy (FT-IR), X-ray diffraction (XRD), excited photoelectron spectroscopy (XPS), confocal laser scanning microscopy, scanning electron microscopy (SEM), atomic force microscopy (AFM), water contact angle, and zeta potential to elucidate the chemical and morphological properties of the membranes modified with the nanoadsorbents. They were then applied to the removal of the toxic metals Pb^{2+}, Cr^{3+}, Cu^{2+}, Ni^{2+}, and Cd^{2+} in multicomponent systems, under batch and dead-end filtration modes of operation. To the best of our knowledge, it is the first time that a salt (PVPI) and a nanoadsorbent (GO) have been incorporated in the hPAN membrane, with their influence on the material's characteristics being systematically studied and related to the performance in removing toxic metals from water.

2. Experimental section

2.1. Chemicals

The chemicals utilized in the preparation of the membranes and the metallic salts employed can be found in Section SD1 of Supplementary Data.

2.2. hPAN/PVPI/GO membranes preparation

2.2.1. Graphene oxide synthesis

The GO was synthesized by pre-oxidation of mineral graphite, followed by oxidation and exfoliation of graphite oxide, as previously described in our work [16], following the modified Hummers methodology [17].

2.2.2. hPAN membrane preparation

The preparation of hPAN membrane was conducted via a phase inversion and alkaline hydrolysis process, as previously described in our work [18], following the Hu *et al.* protocol [19].

2.2.3. Poly(4-vinylpyridine) quaternization

The quaternization of poly(4-vinylpyridine) (PVP) was carried out using the active halide iodomethane, following the methodology developed by Bicak *et al.* [20]. In a 50 mL round-bottom reaction flask, 3.5 g of PVP were dissolved in 16.7 mL of dry dimethylformamide (DMF) under magnetic stirring in a nitrogen atmosphere. Once the polymer had been fully dissolved, 3.15 mL of iodomethane were added dropwise to the mixture. The solution was stirred at room temperature for 24 h, and then filtered with acetone (500 mL) and ethyl ether (500 mL). The solid obtained was collected and dried using a high vacuum pump.

2.2.4. hPAN/PVPI/GO membranes preparation

Following the process used by Halakoo *et al.* [21] to prepare the new membranes using the LbL method, the hPAN membrane was subsequently immersed in (a) a solution of PVPI (1.5 g L^{-1}) for 1 h, (b) deionized water for 3 min, (c) a suspension of GO (1.5 mg L^{-1}) for 1 h, (d) deionized water for 3 min, thus completing the buildup of a bilayer ($hPAN/PVPI_1/GO_1$). The process was repeated for the double-layer ($hPAN/PVP_2/GO_2$) and triple-layer ($hPAN/PVP_3/GO_3$) membranes. For convenience of discussion, the modified membranes have been called A1, A2 and A3, where the numeral refers to the number of PVPI/GO bilayers. To illustrate, Fig. 1 is a schematic of the LbL assembly for membrane preparation.

2.3. Characterization

The water contact angle of the wet membranes was measured using an Attension Optical Tensiometer model Theta Lite, One-Tension program. The measurements were conducted at room temperature with 120 frames captured between 0 and 10 s, with an accurate measurement of 15 μL of water. Contact angle images were obtained at various intervals using a high-speed camera, and the final results were reported as the average of three samples. XRD patterns were obtained at room temperature on a Panalytical XPert Powder XRD instrument, using Cu K-α radiation, operating at 40 kV and 30 mA. The analysis was performed by continuous mode scanning at 2° min^{-1} and 0.02° step in a range of 5° to 100°. XPS spectra were collected using a spectrometer (ScientaOmicron ESCA+) with a hemispherical analyzer (EAC2000), monochromatic Al Kα radiation ($h\nu = 1486.6$ eV) as the excitation source, and a pressure of 10^{-9} Pa. A charge neutralizer (CN10) was used to exclude surface charge

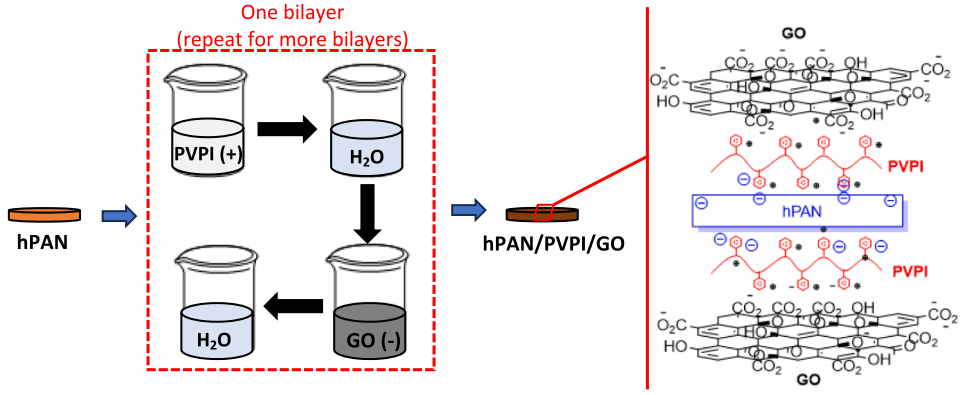

Fig. 1. Schematic representation of the new membranes production.

effects. The XPS high-resolution spectra were recorded at a constant pass energy of 20 eV with 0.05 eV per step for the high-resolution spectra. The energy range analyzed in the survey was between 0.0 and 1200 eV. Data analysis was performed using Casa XPS software. FT-IR analyses were conducted in the range of 4000 to 400 cm^{-1}, using the attenuated total reflection (ATR) method, on a Tensor 27 Bruker FT-IR instrument. Raman spectroscopy analyses were performed on a Horiba Jobin Yvon T64000 coupled to an Olympus BX41 microscope and a charge-coupled device detector. The wavelength of the incident radiation, which differed for each material, was provided by a He-Ne laser (Melles Griot). The laser power was set at 1 mW in the sample compartment, and the spectral resolution was 2 cm^{-1}. Scanning electron microscopy (SEM) was performed on a Tescan instrument (Vega 3 SEM) with high resolution, operated at 30 kV and a scan spacing of 180 nm. The sample sections were affixed vertically and horizontally to a surface with double-sided carbon adhesive and then vacuum sprayed with an ultra-thin gold film. Atomic force microscopy (AFM) was conducted on a NanoWizard4 instrument, JPK, with a resonance frequency of 150 kHz and a constant nominal force of 0.7 N m^{-1}, with a 512 × 512 pixel resolution. Image processing and statistical calculations were carried out using Gwyddion software. The flux of the membranes (L $m^{-2}h^{-1}$) was evaluated by measuring the pure water flux in a membrane effective area of 12.56 cm^2 under a transmembrane pressure difference of 700 mmHg. The average surface charge of the membranes at different pH was determined by zeta potential analysis using a Malvern ZetaSizer Nano series DLS ZEN3600. The membranes were cut into small pieces and submerged in solutions with different pH ranges at 25 °C. 0.1 M NaOH and 0.05 M HCl were used to adjust the pH during the measurements.

2.4. Metal ions removal by new membranes

2.4.1. Batch adsorption assays

For the batch adsorption assays, initially, 20 mL of a synthetic contaminant solution containing the five metals were prepared with estimated concentrations based on quantifications carried out on industrial effluents [22–24] (Cd^{2+}: 1.8 mg L^{-1}, Ni^{2+}: 4.9 mg L^{-1}, Cu^{2+}: 4.1 mg L^{-1}, Cr^{3+}: 12.2 mg L^{-1} and Pb^{2+}: 10.2 mg L^{-1}). Subsequently, a 0.05 g membrane unit was then added to the contaminant solution.

The system was then placed in an orbital shaker (LABWIT – Shaker Incubator ZWYR-240) at 180 rpm and room temperature for 24 h. At the end, aliquots were taken, acidified, and diluted, and then analyzed in an atomic absorption spectrophotometer (GBC, Avanta PM). The dilution factors are listed in Table SD2 in Supplementary Data.

The solid concentration or solid loading (q_i, mg g^{-1}, Eq. (1) and the removal efficiency (%, Eq. (2) were calculated from the measured readings. The solid concentration represents the mass of metal removed per unit mass of membrane:

$$q_i = \frac{(C_{i,0} - C_{i,f})V}{m} \quad (1)$$

where $C_{i,0}$ and $C_{i,f}$ (mg L^{-1}) are the initial and final metal concentrations in solution, respectively, V (L) is the solution volume, and m (g) is the mass of the membrane. Under equilibrium conditions (reached in 24 h), Eq. (1) gives the equilibrium solid concentration, $q_{i,e}$ (mg g^{-1}). The removal efficiency (%, Eq. (2) refers to the percentage of metal that was adsorbed on the membrane, *i.e.*, that was uptaken from the initial solution.

$$\text{Removal efficiency} = 100 \times \frac{C_{i,0} - C_{i,f}}{C_{i,0}} \quad (2)$$

The selectivity of a membrane towards ion i relative to ion j $(S_{i,j})$ in a multicomponent mixture can be estimated dividing both distribution coefficients, K:

$$S_{i,j} = \frac{K_i}{K_j} = \frac{q_i/C_i}{q_j/C_j} \quad (3)$$

2.4.2. Dead-end filtration assays

For the semi-continuous dead-end filtration adsorption assays, a synthetic solution containing the five metals was initially prepared using the estimated concentrations of real effluents mentioned in section 2.4.1. Subsequently, the solution permeated the membranes with an effective area of 12.56 cm^2 under 700 mmHg vacuum in a filtration system. At the end, aliquots of the obtained permeate (filtrate) were collected, acidified, diluted, and then analyzed by atomic absorption spectrophotometry as in section 2.4.1. The measured values were employed to calculate the removal efficiency (%, Eq. (2) and the final solid concentration (q_i, mg g^{-1}, Eq. (1).

3. Results and discussion

3.1. Characterization

3.1.1. Graphene oxide and poly(4-vinylpyridinium iodide)

3.1.1.1. Raman spectroscopy. The Raman spectrum of the synthesized GO is shown in Fig. 2(a). A typical Raman spectrum of GO is characterized by a G band at 1600 cm^{-1}, which is related to the E_{2G} vibrational mode for sp^2 hybridized carbon atoms strongly coupled to hexagonal layers, and a D band at 1350 cm^{-1}, which is associated with the presence of defects in the hexagonal structure. The intensity ratio between the two bands (I_D/I_G) indicates material disorder. For GO, this ratio is close to 1 [25].

Concerning the synthesized GO, the vibrational mode of the G band is observed at 1594 cm^{-1} and the D band at 1332 cm^{-1}. The value of the

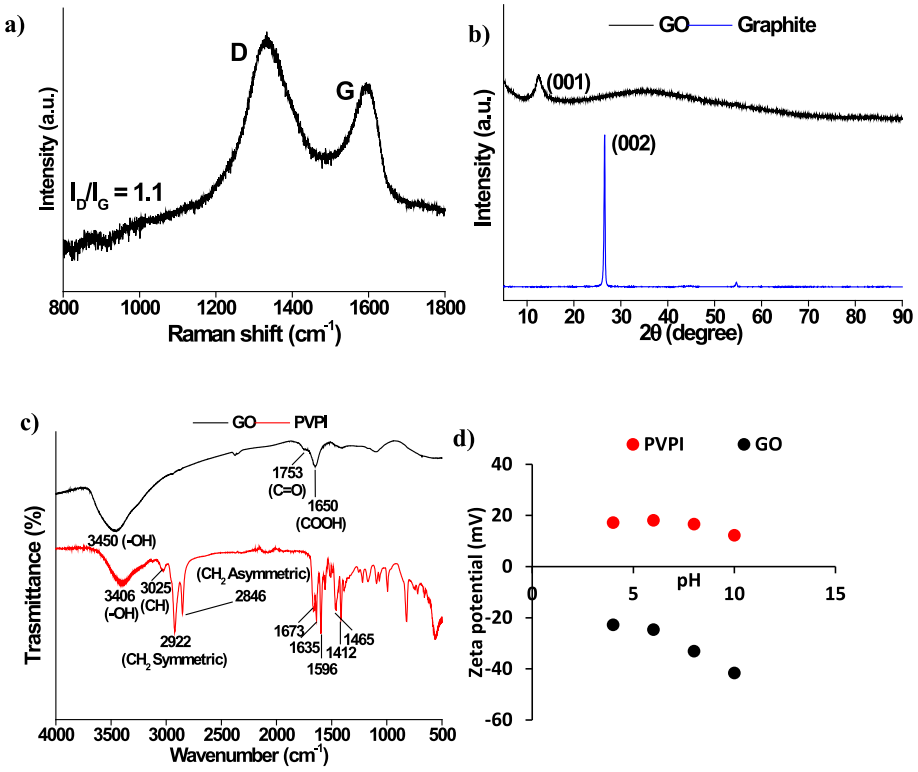

Fig. 2. **(a)** GO Raman spectrum. **(b)** XRD patterns of GO (black line) and mineral graphite (blue line). **(c)** FT-IR spectra of GO (black line) and PVPI (red line). **(d)** Zeta potential of GO (black circle) and PVPI (red circle).

calculated I_D/I_G ratio was equal to 1.10, confirming the success of the GO synthesis.

3.1.1.2. X-ray diffraction. The mineral graphite and GO samples were subjected to XRD analysis, and the results are presented in Fig. 2(b). The XRD pattern of the mineral graphite exhibits one peak at 26.62°, which corresponds to the 002 crystallographic plane. In contrast, the XRD pattern of the synthesized GO shows a dominant peak at 12.38°, which is associated with the 001 crystallographic plane. Applying Bragg's law to both patterns, the interlayer spacing of mineral graphite and GO was found to be 0.34 and 1.01 nm, respectively [26]. The increase in interlayer spacing observed for GO compared to graphite indicates that there have been ruptures in the crystalline structure of the latter, suggesting the insertion of oxygenated groups into the nanomaterial [27].

3.1.1.3. Fourier transform infrared spectroscopy. Fig. 2(c) depicts the FT-IR spectra of GO and PVPI. The spectrum of GO indicated the oxidation of the nanomaterial, as evidenced by the presence of bands at 3450, 1753, and 1650 cm^{-1}. These bands are attributed to the presence of OH, ketones (C=O), and carboxyl groups, respectively. In the spectrum of PVP quaternized with iodomethane, the absorption band at 3025 cm^{-1} corresponds to unsaturated bonds of C-H units [28], while the bands at 2922 and 2846 cm^{-1} refer to the symmetric and asymmetric stretching of the methylene group (CH_2) of the polymer, respectively [29]. In addition, the absorption bands at 1596, 1465, and 1412 cm^{-1} correspond to the C=C and C=N vibrations of the pyridine ring [30]. These absorption peaks indicate the presence of pyridine rings in the structure. Moreover, a comparison of the observed spectra with those reported in the literature [31] indicates that the bands and transitions observed at 1673 and 1635 cm^{-1} in the spectrum of the material can be attributed to the PVP^{n+} cation. This evidence supports the conclusion that the quaternization of PVP was successful.

3.1.1.4. Zeta potential. The zeta potential of the GO and PVPI suspensions was measured in the pH range of 4–10 and the results obtained are shown in Fig. 2(d). According to the analysis, GO has a negative surface charge, while PVPI has a positive surface charge in the evaluated pH range. PVPI exhibited zeta potential values ranging from + 17.3 to + 12.3 mV, and GO showed values from –22.7 to –41.6 mV when pH varied from 4 to 10.

The negative surface charge of GO is associated with the presence of oxygenated groups, such as carbonyl, hydroxyl, and epoxy, in the basal plane and at the edges of the sheets [18]. This result indicates the presence of a highly oxidized graphene derivative, suggesting the successful synthesis of the nanoadsorbent. Similarly, the positive surface charge of PVPI indicates the quaternization of the PVP polymer with iodomethane. The insertion of the alkyl halide into the polymer forms a quaternary ammonium cation [20].

It can also be argued that the excess of OH^- in the medium at increasing pH increases the negative charge of GO and decreases the positive charge of PVPI, due to the deprotonation of the oxygenated functions in the nanoadsorbent and the interactions of the ions with the quaternary amine of the salt, respectively [16]. Therefore, for the LbL assembly of the hPAN/PVPI/GO membranes, the PVPI and GO dispersions were prepared at pH 6, as this provides a good compromise among a mild pH and a greater interaction between the materials and the pristine membrane.

3.1.2. hPAN/PVPI/GO membranes

3.1.2.1. X-ray diffraction and Fourier transform infrared spectroscopy. XRD patterns of the hPAN membrane and the hPAN/PVPI/GO membranes with 1, 2, and 3 bilayers of PVPI/GO are presented in Fig. 3(a). The XRD pattern of the hPAN membrane exhibits a minor sharp peak at approximately 16.8°, which can be attributed to the crystal plane (1 0 0) and is indicative of the presence of nitrile groups in the polymer structure [32]. Additionally, there is a broad band at 23.0°, which can be attributed to the amorphous region of the membrane [33].

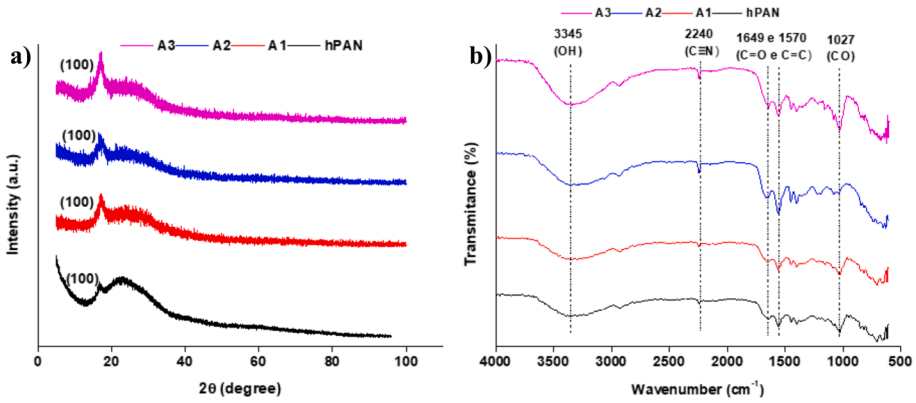

Fig. 3. **(a)** XRD patterns of hPAN membrane and hPAN/PVPI/GO membranes with different PVPI/GO bilayers. **(b)** FT-IR spectra of hPAN membrane and hPAN/PVPI/GO membranes with different PVPI/GO bilayers.

In the membranes containing different bilayers of PVPI/GO (Fig. 3 (a)), although the crystalline plane (001) of GO (Fig. 3(b)) is not observed, their XRD patterns are similar to those of the pristine hPAN membrane. The presence of the nanoadsorbent in the new membranes may be related to the significant reduction of the broad amorphous band of membranes A1, A2, and A3. The absence of the characteristic GO peak in the composite membranes may be attributed to the low GO mass attached to the polymer matrix's surface [32], or even to its inhomogeneous deposition on the hPAN. As the XRD technique is used to analyze the surface of materials [34], and since the PVPI/GO layers are not homogenously dispersed on the surface of the pristine membrane, the X-ray beam of the equipment may have scanned a sample band with a low material content. A similar observation was reported by Hung et al. [35] when preparing GO membranes on a modified PAN substrate by the pressure-assisted self-assembly technique. While the nanoadsorbent exhibited an XRD pattern with a diffraction signal at 26.25°, this peak was absent in the diffractogram of the GO/PAN membrane [35].

Fig. 3(b) shows the FT-IR spectra of the hPAN membrane and the hPAN/PVPI/GO membranes with 1, 2, and 3 bilayers of PVPI/GO. The FT-IR spectrum of the hPAN (Fig. 3(b)) substrate was corroborated by the appearance of a broad absorption band at 3345 cm^{-1}, small bands at 1649 and 1570 cm^{-1}, and a narrow band at 1027 cm^{-1}. These bands are attributed to the stretching of the hydroxyl, carbonyl, and C-O groups, respectively [36]. The sharp band at 2240 cm^{-1} corresponds to the nitrile group (C≡N), which remains present in the membrane, indicating partial hydrolysis of the material [37].

The absorption bands characteristic of hPAN are present in the spectra of the membranes incorporated with PVPI/GO, although the progressive increase of the layers has led to changes in the intensity and shape of the peaks. In membranes A1, A2 and A3, the bands corresponding to oxygenated functions at 3345, 1649/1570, and 1027 cm^{-1} exhibited an increase in intensity relative to those of the hPAN membrane. These alterations in the spectral bands of the membranes incorporated with PVPI/GO may suggest the presence of intermolecular hydrogen bonds between the oxygenated functions of GO and the functional groups of the hPAN, indicating the presence of GO on the surface of the material. Similar conformations were also observed by Jauhari et al. [38] in the synthesis of fibers composed of GO and polyacrylonitrile.

3.1.2.2. X-ray photoelectron spectroscopy. Table 1 and Fig. 4 summarize the survey analyses and the high-resolution C1s and N1s spectra of the hPAN, A1, A2, and A3 membranes, respectively. The analysis of the tabulated data (Table 1) reveals that all the membranes include the same main elements, with C, O, N, and Na, with a divergence in the abundance of each one. The hPAN membrane has 75.8 % and 11.9 % of C and N,

Table 1
Scanning data obtained for the membranes by XPS analysis.

Membrane	Content (%)				
	C	O	N	Na	I
hPAN	75.8	12.1	11.9	0.2	–
A1	75.5	22.6	1.5	0.4	0
A2	76.1	21.9	1.7	0.3	0
A3	78.7	18.9	2.1	0.3	0

respectively, associated with the polymer. Additionally, 12.1 % of O is present, which is related to the partial hydrolysis of the material. Furthermore, the presence of Na (0.2 %) is associated with the alkaline hydrolysis of the membrane with NaOH. In other studies, these proportions were comparable to those of the hydrolyzed PAN polymer [39]. For the composite membranes, a significant variation can be observed between their oxygen and nitrogen contents in comparison to those of the pristine membrane. Regarding O, the incorporation of GO on the pristine polymer resulted in an increase in the element content, with values varying from 12.1 % in hPAN to 22.6 %, 21.9 %, and 18.9 % for the A1, A2, and A3 membranes, respectively. Regarding N, there was a decrease in the element content in the modified membranes, with hPAN exhibiting 11.9 % of the element, while the A1, A2, and A3 membranes showed a variation of 1.5 %, 1.7 %, and 2.1 %, respectively. The surface of the pristine membranes was coated with PVPI/GO, resulting in an increase in C and O content of the material, with a corresponding decrease in N content. However, it was still possible to observe that, albeit lower than in the hPAN membrane, there was an increase in N content from the A1 to the A3 membrane. These results indicate (1) the incorporation of GO on the modified membranes, due to the increase in O content in the materials, and (2) the increase in PVPI in the materials, due to the progressive increase in N content.

The high-resolution C1s XPS spectra for the hPAN membrane (Fig. 4 (a)) exhibit peaks centered at 284.7 eV (39.2 %), 285.8 eV (21.4 %), 286.9 eV (30.5 %), 287.7 eV (7.2 %), and 288.7 eV (1.7 %), corresponding to the C-sp^3/C-sp^2, C-N, C-O, C=O/N-C=O, and COOH bonds, respectively [40]. For the GO-modified membranes, the high-resolution C1s spectra (Fig. 4(b)-(d)) exhibit similarities to the spectrum of the pristine membrane, with the exception of the disappearance of the peak corresponding to the C-N bonds and variations in the intensities of the other peaks. The disappearance of the C-N bond signal in membranes A1, A2, and A3 may be attributed to the overlapping of the nitrile and amine groups of hPAN and PVPI, respectively, by the long carbon chain of GO. This may be due to possible electrostatic interactions between the PVPI quartenary amine and the nanoadsorbent oxygen functions [16]. Moreover, the variations in the intensities of the peaks present in the modified membranes indicate an increase in the relative area of the peaks associated with the oxygenated functions, which is accompanied

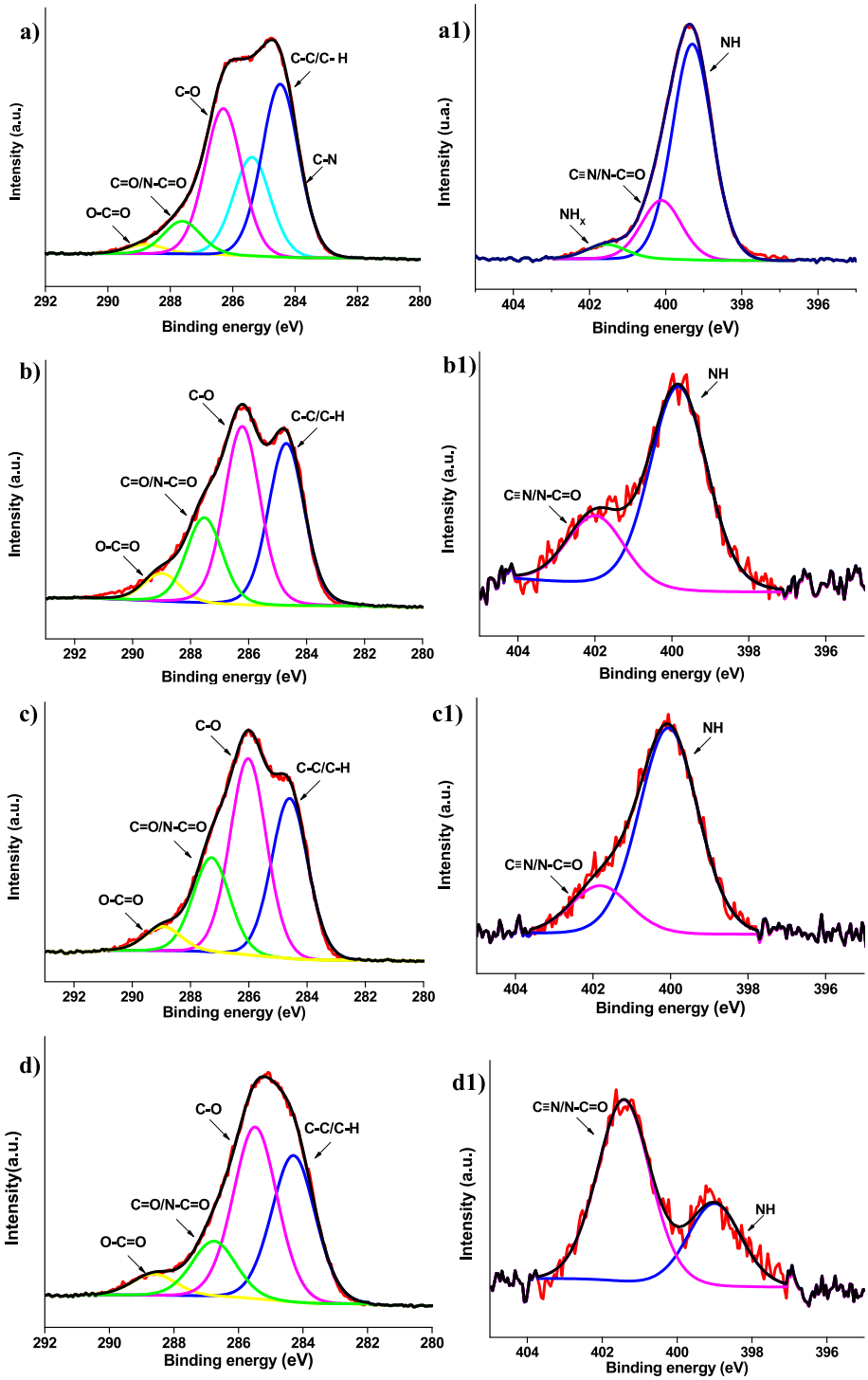

Fig. 4. High-resolution XPS spectra: **(a)** C1s from hPAN, **(a1)** N1s from hPAN, **(b)** C1s from A1, **(b1)** N1s from A1, **(c)** C1s from A2, **(c1)** N1s from A2, **(d)** C1s from A3 and **(d1)** N1s from A3.

by a decrease in the peaks related to the C-C bonds. These results suggest the incorporation of GO into the matrix, given that the nanoadsorbent is rich in oxygenated organic functions [18].

The high-resolution N1s XPS spectra for the hPAN membrane (Fig. 4 (a1)) show peaks centered at 399.5 eV (78.1 %), 400.3 eV (17.7 %), and 401.9 eV (4.2 %), which can be attributed to the NH, C≡N/N-C=O, and NH_X bonds, respectively [41]. The high-resolution N1s XPS spectra of the GO-modified membranes (Fig. 4(b1)-(d1)) exhibit similarities to the pristine membrane spectra, except for the disappearance of the peak corresponding to the NH_X and variations in the intensities of the other peaks. The disappearance of the NH_X signal for the new A1, A2, and A3 membranes and the increase in the peak related to N-C=O bonds (corresponding to the increase in GO content in the membranes) are associated with the rise of oxygenated organic functions in hPAN [18]. As observed by Péres-Álvarez *et al.* [40], an increase in O content in the polymer matrix triggers a decrease in N content, resulting from the loss of cyano groups to form carboxylic groups.

3.1.2.3. Morphological properties. High depth images of the membrane surface (Fig. 5(a)-(d)) were obtained using laser scanning confocal

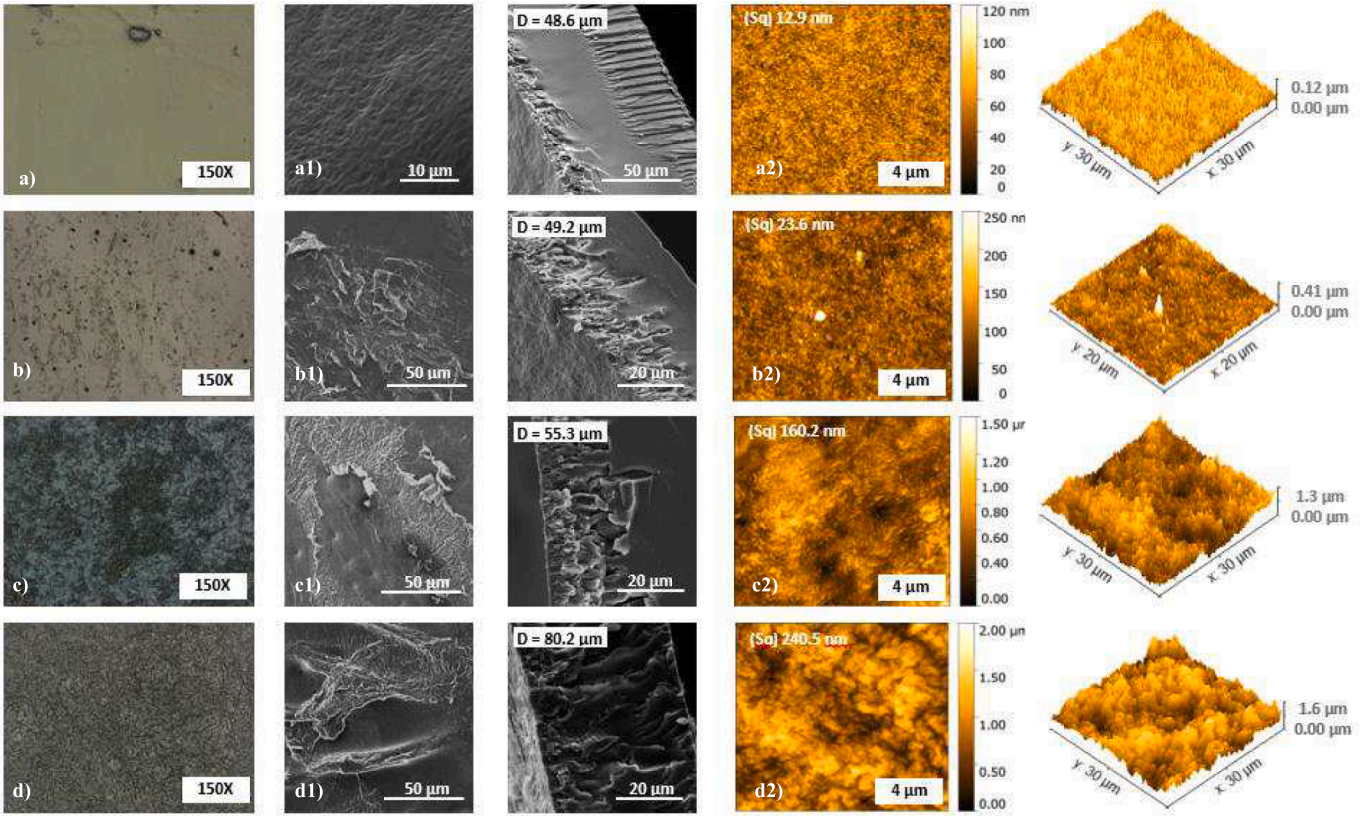

Fig. 5. Confocal images of the dried membrane surfaces **(a)** hPAN, **(b)** A1, **(c)** A2, and **(d)** A3. SEM images of the surfaces and cross sections of the **(a1)** hPAN, **(b1)** A1, **(c1)** A2, and **(d1)** A3 membranes. AFM images of **(a2)** hPAN, **(b2)** A1, **(c2)** A2, and **(d2)** A3 membranes.

microscopy and show relevant differences between the GO-containing membranes and hPAN. The hPAN (Fig. 5(a)) membrane has a dense and smooth surface. The A1 membrane (Fig. 5(b)) also has a dense, smooth surface, with pores and thin ribbing on the pristine polymer. The images of the A2 (Fig. 5(c)) and A3 (Fig. 5(d)) membranes demonstrate that the smooth surface of the material has been replaced by a rough surface covered by materials, which are likely to be related to the presence of PVPI/GO attached to the polymer surface. In accordance with the confocal laser scanning microscopy, the SEM images of the membranes indicate surface variations in the materials according to the increase of PVPI/GO on the pristine polymer.

Fig. 5 (a1)-(d1) show the surface morphology and cross-section of the hPAN, A1, A2, and A3 membranes obtained by SEM analysis. Generally, an increase in PVPI/GO on hPAN resulted in an increased incidence of defects on the surface and in the underlying layer of the membranes. SEM images of the surface of the materials show that while hPAN (Fig. 5 (a1)) exhibits a dense and rough surface layer, membranes A1 (Fig. 5 (b1)), A2 (Fig. 5(c1)), and A3 (Fig. 5(d1)) display the presence of material deposited on their surfaces. Furthermore, the higher the PVPI/GO content on the material, the more these materials agglomerated, taking on the shape of thin ribbings. In addition to the changes observed in the membrane surface, the increase in the content of materials in the polymer matrix also affected the morphology of the cross-section of the materials. The hPAN membrane has three distinct regions: a uniform and denser layer in the center, surrounded by two porous layers, one of which resembles a stack of overlapping slabs. The membranes A1 and A2 exhibit two regions: a porous layer with irregular finger-like macrovoids and a uniform layer. The membrane A3, on the other hand, only shows a porous cross-section area with irregular finger-like macrovoids.

These results indicate that the deposition of successive bilayers of PVPI/GO progressively modifies the morphology of the supporting hPAN membrane. The modifications are not only observable on the surface but also significantly and gradually extend to the interior of the membranes, which will increase the interaction with the pollutants solutions under static or permeation conditions [42]. Similar results were obtained by Januário *et al.* [13] in the preparation of polyethersulfone membranes modified with sulfuric acid, titanium dioxide (TiO_2), and GO solutions by the LbL assembly methodology. The authors observed that the TiO_2 nanoparticles were irregularly distributed and agglomerated on the membrane surface. They attributed this phenomenon to complete inhomogeneity of the nanoparticle solution in the ultrasonic stage and the subsequent agglomeration of the nanoparticles with GO on the polymer surface due to electrostatic interaction.

The thickness of the hPAN, A1, A2, and A3 membranes was also measured by SEM analysis, with average lengths of 48.56, 49.22, 55.34, and 80.25 µm, respectively, indicating that their thickness increases with the number of PVPI/GO bilayers adhered to the polymer. These results were expected since variations in the thickness of composite membranes are common in LbL assembly processes [13].

AFM analyses were also conducted to assess not only the morphological surface properties of the membrane but also to evaluate the three-dimensional profile of the materials. Fig. 5(a2)-(d2) summarize the images and three-dimensional profiles obtained from the analysis of the hPAN, A1, A2, and A3 membranes. The hPAN membrane (Fig. 5(a2)) exhibits low surface roughness, with a mean square roughness index (Sq) estimated at 12.9 nm. In contrast, these characteristics were modified for the membranes containing GO and PVPI. Membranes A1 (Fig. 5(b2)), A2 (Fig. 5(c2)), and A3 (Fig. 5(d2)) exhibit higher surface roughness, which increased as PVPI/GO adhered to the hPAN surface. Their Sq was found to be 23.6, 160.2, and 240.5 nm, respectively, according to the number of layers of PVPI/GO on the pristine polymer (1, 2, and 3). The results demonstrate that the addition of PVPI/GO to the membrane increases the surface roughness of the pristine polymer. Januário *et al.* [43] stated that the apparent surface defects on the

membrane surface and the increase in the roughness of materials modified with GO by the LbL assembly method are due to the folding effect of the GO nanosheets during the process.

Water contact angle.

In order to have information about the hydrophilicity of the novel membranes in comparison to the pristine polymer, contact angle measurements with water were conducted on hPAN, A1, A2, and A3, and the results obtained are shown in Table 2. According to the analysis, a hydrophobic surface has a static contact angle greater than 90°, whereas a hydrophilic surface has an angle less than 90° [44]. The results for all the membranes analyzed were less than 90°, with values ranging from 7.58° to 17.70°. This indicates that the materials have a hydrophilic nature with a suitable wetting surface.

Although all the membranes have a hydrophilic surface, the pristine hPAN polymer (7.58°, Table 2) had a contact angle approximately 1.5 times lower than the A1 membrane (12.32°, Table 2), which is the lowest contact angle with water among the modified membranes. This discrepancy in contact angle between the pristine polymer and the modified membranes may be related to the morphological characteristics and chemical composition of hPAN. As mentioned above, the pristine membrane exhibits macropores/defects near the surface, which contributes to the penetration of water from the surface to the interior of the membrane by capillary action of the hydrophilic porous media [45]. Regarding the chemical composition of the membrane surface, the partial hydrolysis of the nitrile functions of PAN results in the generation of hydrophilic COO^- and $CONH_2$ functional groups in the membrane matrix, thereby enhancing the hydrophilic character of the material [45].

The membranes containing the cationic polymer and the anionic nanoadsorbent (A1, A2, and A3) exhibited an increase in the water contact angle with the increase in PVPI/GO layers on hPAN. The values obtained were 12.32°, 13.61°, and 17.70° for membranes A1, A2, and A3, respectively. These results may be attributed to the presence of GO and PVPI on the surface of the membranes, which have hydrophobic and hydrophilic zones in their structure, respectively. Assuming that the nanoadsorbent adheres to the membrane surface through electrostatic interactions with the cationic polymer PVPI [15], the hydrophobic centers of GO become more accessible for interaction with the medium, resulting in an increase in the water contact angle of membranes with higher nanoadsorbent content. Similar results were obtained by Mokkapati *et al.* [46], who stated that high concentrations of GO can cause an increase in the water contact angle due to the GO nanosheets having hydrophobic fractions that can be more exposed on the membrane surface.

3.1.2.4. Pure water flux. The results of the pure water flux for the hPAN, A1, A2, and A3 membranes are presented in Fig. 6. Equivalent results were obtained for the metal solution. The findings indicate that the flux decreased as the PVPI/GO content on the surfaces of the pristine polymer increased. This suggests that GO and PVPI have attached to the hPAN surface. The hPAN membrane exhibited the highest flux, 170.8 L $m^{-2}h^{-1}$, followed by the A1, A2, and A3 membranes with fluxes of 63.0, 56.5, and 45.9 L $m^{-2}h^{-1}$, respectively. This reduction in water flux through the membranes with an increasing number of bilayers of PVPI/GO deposited over the hPAN is associated with morphological and physicochemical changes in the pristine polymer.

Regarding membrane morphology, hPAN has greater total macropores/defects than the modified membranes. These features contribute to greater permeation of water through the material [18]. Furthermore, the hydrophilic functional groups increase membrane wettability (Table 2) and affinity towards water molecules, which may facilitate their transport through the hPAN membrane matrix [47].

The accumulation of PVPI and GO over the surface of the pristine polymer resulted in an increase in the mean square roughness of the modified membranes (A1, A2, and A3), as well as a decrease in the total macropores/defects volume of these materials with eventual pore blockage. This morphological change in the membranes, in turn, increases the flow resistance, making it difficult for water to pass through [48]. Furthermore, the PVPI/GO contributes to a small reduction of the surface hydrophilicity of the modified membranes in comparison to the hPAN membrane (Table 2), which may slightly penalize their affinity towards the water molecules [18].

3.1.2.5. Zeta potential. The zeta potential of the hPAN, A1, A2, and A3 membranes was measured at pH 6, and the results obtained are presented in Fig. 7. The analysis revealed that, despite all the materials exhibit a negative surface charge, the negative potential of the membranes decreased as the bilayers of PVPI/GO adhered to the material increased. The zeta potentials of the hPAN, A1, A2, and A3 membranes were –23.4, −21.7, −16.4, and −12.8 mV, respectively.

The negative surface charge of hPAN is attributed to the presence of oxygenated functions such as carboxyl and amide in the polymer matrix, resulting from the alkaline hydrolysis of the material [49]. Regarding the membranes coated with different layers of PVPI/GO, while the

Table 2
Water contact angle of hPAN, A1, A2 and A3 membranes.

Membranes	Contact angle (θ°) at 10 s	Images of the contact angle at different times 0.1 s	3 s	10 s
hPAN	7.58	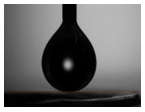		
A1	12.32	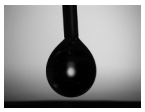		
A2	13.61			
A3	17.70			

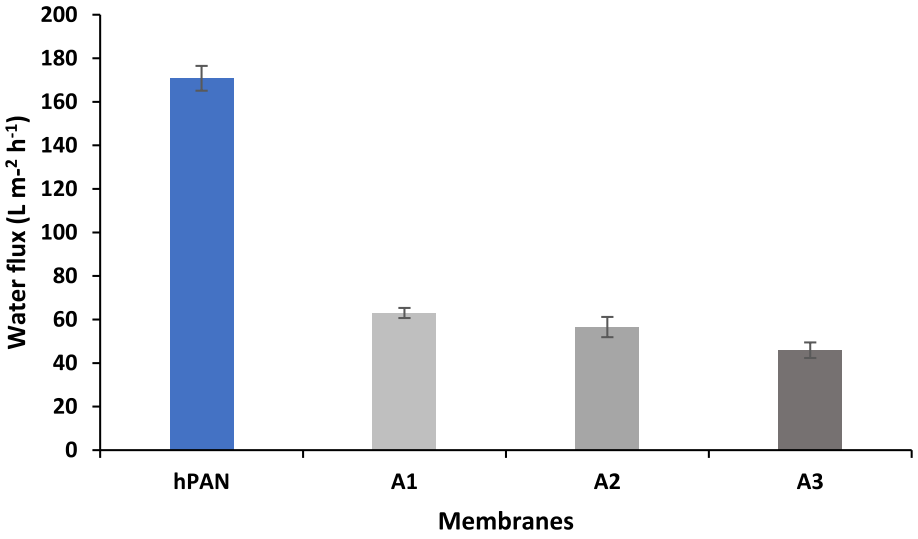

Fig. 6. Flux of pure water through hPAN, A1, A2 and A3 membranes.

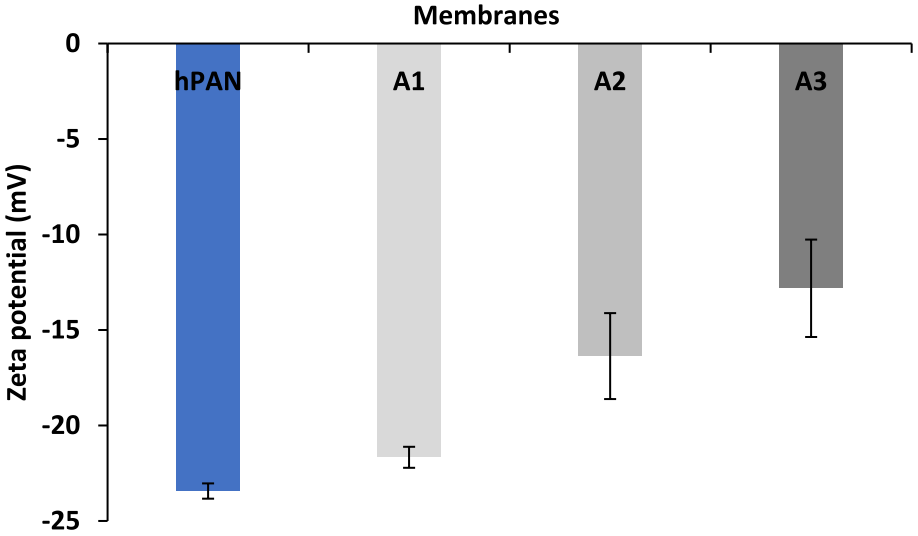

Fig. 7. Zeta potential of hPAN, A1, A2 and A3 membranes.

negative surface charge of the composite membranes was also evident, the decrease of their absolute charge with increasing cationic polymer and anionic nanoadsorbent indicates the influence of PVPI on the surface.

In the development of the new membranes, the cationic PVPI polymer was used as an electrostatic attracting agent between the anionic materials, GO and hPAN. Consequently, PVPI, as a quaternary amine, contributes to a positive surface charge [20] (Fig. 2(d)). The reduction in the negative charge of the surface membranes with increasing layers of PVPI and GO in hPAN indicates that the deposition of PVPI, in addition to acting as an electrostatic attracting agent, results in an increase of the positive charges at the membrane surface [39].

3.2. Adsorption of toxic metals in multicomponent systems

The hPAN, A1, A2, and A3 membranes were subjected to metal ion adsorption in batch and dead-end filtration processes. In this stage of the study, the main objective was to evaluate the impact of the modifications resulting from the addition of PVPI/GO on the adsorptive and filtering potential of the membranes.

3.2.1. Batch adsorption study

The use of membranes in batch adsorption experiments offers a significant advantage: the adsorbent can be easily removed from the aqueous medium after the adsorption process, eliminating the need for filtration, which makes the purification process more expensive. Therefore, batch assays to study the adsorption potential of the membranes for contaminants in water were performed using a complex system containing the metal ions: Cd^{2+}, Ni^{2+}, Cu^{2+}, Cr^{3+}, and Pb^{2+}. The results obtained are shown in Fig. 8.

The results of the experiments (Fig. 8) indicate that the modified membranes exhibited a higher removal potential than the hPAN membrane. This suggests that the incorporation of PVPI/GO led to an improvement of the adsorption performance of the pristine polymer, which may be attributed to the presence of OH and COOH groups in GO, which are likely to form coordination complexes with metal ions [50]. Among the membranes analyzed, A3 showed the highest removal ability (and solid loadings) with measured values of 6.6 % ($q_e = 0.05$ mg g^{-1}), 23.1 % ($q_e = 0.45$ mg g^{-1}), 50.4 % ($q_e = 0.83$ mg g^{-1}), 64.3 % ($q_e = 3.14$ mg g^{-1}), and 99.9 % ($q_e = 4.08$ mg g^{-1}) for Cd^{2+}, Ni^{2+}, Cu^{2+}, Cr^{3+}, and Pb^{2+} ions, respectively. Moreover, from the data presented in Fig. 8, it can be concluded that all membranes showed a higher

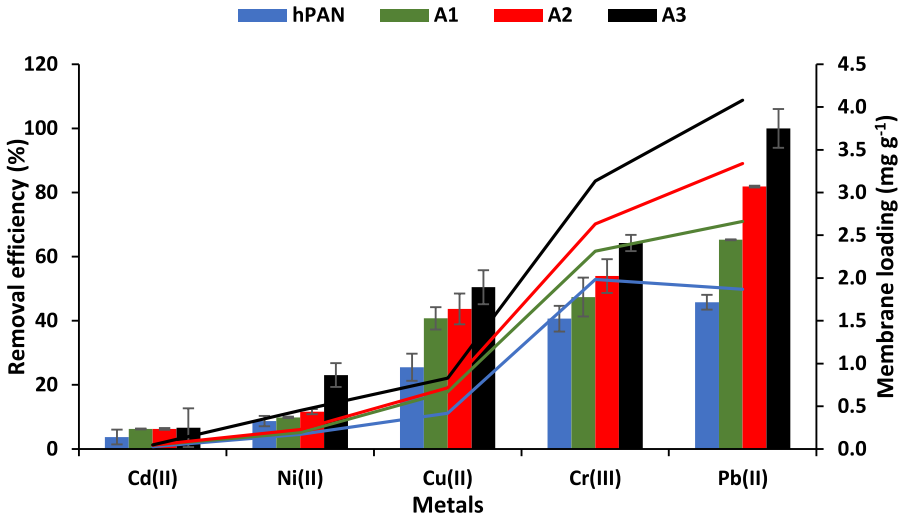

Fig. 8. Toxic metals batch adsorption by hPAN (blue), A1 (green), A2 (red) and A3 (black) membranes. Bars represent removal efficiency, and lines show pollutants concentration in membranes. Membrane mass of 0.05 g, solution volume of 20 mL, initial concentrations of Cd^{2+} of 1.8 mg L^{-1}, Ni^{2+} of 4.9 mg L^{-1}, Cu^{2+} of 4.1 mg L^{-1}, Cr^{3+} of 12.2 mg L^{-1}, and Pb^{2+} of 10.2 mg L^{-1}, adsorption time of 24 h, agitation of 180 rpm, pH 5.5, and room temperature.

selectivity for Pb^{2+}, Cr^{3+}, and Cu^{2+} ions compared to Ni^{2+} and Cd^{2+} ions. This is clearly emphasized by the calculated selectivities relative to Cd^{2+} using Eq. (3), which, for membrane A3, were 13450, 24.2, 13.7, 4.0, and 1.0, respectively. The detailed calculations are available in Sections SD4 and SD5 in Supplementary Data.

With regard to membrane selectivity, as elucidated by Upreti *et al.* [51], this variation in cation removal potential can be attributed to the chemical interaction between metal ions and adsorbent materials, which depends on the affinity of the contaminants to interact with the functional groups of the adsorbent. In the case of porous materials, steric limitations associated with ion size can also affect adsorption. In that study [51], the authors observed that the affinity of As^{5+} ions was lower than that of Pb^{2+} with respect to the adsorbent. These results may be related to the radius and charge density of the ions, their coordination numbers (number of hydration molecules) and hydration energies, which globally favored Pb^{2+} adsorption [52,53].

For equivalent valences, larger ions in solution may interact more strongly with solid sorbents due to the weaker hydration forces that retain water molecules around them [54]. Given that the ionic radii of the metals studied in this essay can be roughly ordered as $Pb^{2+} > Cd^{2+} > Cr^{3+} \cong Cu^{2+} \cong Ni^{2+}$, such reasoning only fails for the predicted selectivity of Cd^{2+} ions. Computer simulations may be used to unveil this behavior.

3.2.2. *Semi-continuous dead-end filtration adsorption study*

The removal efficiency of the membranes by dead-end filtration was explored with a mixed aqueous system containing the metal ions: Cd^{2+}, Ni^{2+}, Cu^{2+}, Cr^{3+}, and Pb^{2+}. The removal efficiency and solid concentration of the membranes are shown in Fig. 9.

An analysis of the results (Fig. 9) shows that the modified membranes had a greater removal potential than the pristine hPAN membrane, which was even more evident than in the batch assays. Consequently, the deposition of PVPI/GO on the pristine hPAN membrane resulted in a notable enhancement of the adsorption performance of the materials in

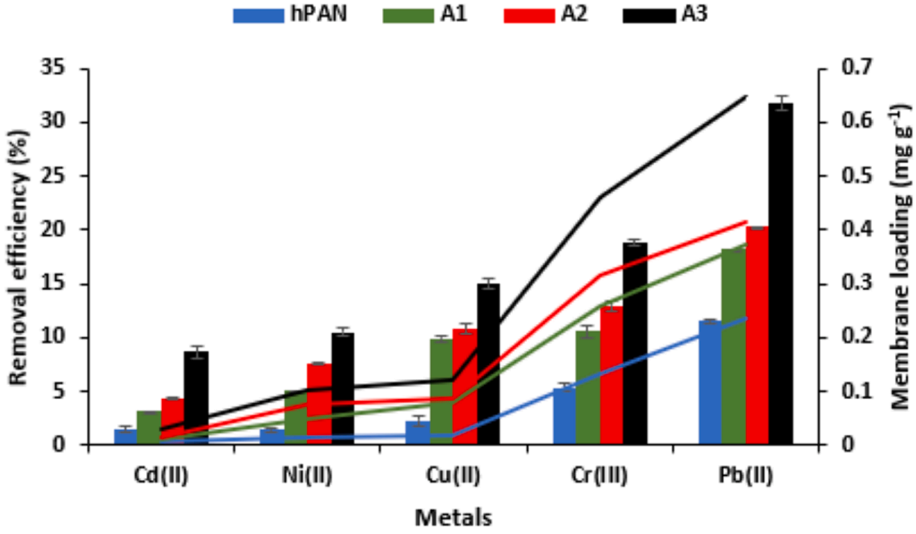

Fig. 9. Toxic metals removal by dead-end filtration using hPAN (blue), A1 (green), A2 (red) and A3 (black) membranes. Bars represent removal efficiency, and lines show pollutants concentration in membranes. Membrane effective area of 12.56 cm^2, percolated volume of 20 mL, initial concentrations of Cd^{2+} of 1.8 mg L^{-1}, Ni^{2+} of 4.9 mg L^{-1}, Cu^{2+} of 4.1 mg L^{-1}, Cr^{3+} of 12.2 mg L^{-1}, and Pb^{2+} of 10.2 mg L^{-1}, filtration time of 5–20 min, pump pressure at 700 mmHg, pH 5.5, and room temperature.

batch and filtration systems. The A3 membrane, which exhibited the highest removal percentages (and solid loadings) among those analyzed, attained values of 8.7 % ($q = 0.03$ mg g^{-1}), 10.5 % ($q = 0.10$ mg g^{-1}), 15.0 % ($q = 0.12$ mg g^{-1}), 18.8 % ($q = 0.46$ mg g^{-1}), and 31.8 % ($q = 0.65$ mg g^{-1}) for Cd^{2+}, Ni^{2+}, Cu^{2+}, Cr^{3+}, and Pb^{2+}, respectively. The detailed calculations are available in Section SD4 in Supplementary Data.

While in the batch assays the removal percentages of the A3 membrane for metal ions were 6.6 %, 23.1 %, 50.4 %, 64.3 %, and 99.9 % for Cd^{2+}, Ni^{2+}, Cu^{2+}, Cr^{3+}, and Pb^{2+}, respectively, in the filtration system, the respective values for the same membrane and metals were generally much inferior: 8.7 %, 10.5 %, 15.0 %, 18.8 %, and 31.8 %. The same happened with the solid loadings, q_i. In the batch system, the membranes were maintained in contact with the multicomponent solution for 24 h, while in the dead-end filtration mode the contact times between the adsorbent and permeating solution were only a few minutes. Such low contact times reduce the mass transfer efficiency between the adsorbent and adsorbate due to the rate-controlled nature of membrane separations. On the contrary, the long batch experiments of section 3.2.1 corresponded to equilibrium stage operations.

In a porous membrane containing macropores/defects under dead-end filtration, the separation may involve the following steps: (1) convective transport of solution through macropores/defects by viscous flow; (2) intraparticle transport of the solutes from the bulk of the solution inside the pores to their walls; (3) intraparticle diffusion (in series and in parallel) through the micro/mesopores and/or dense phase of the membrane; (4) interaction with the active sites of the adsorbent. Consequently, the contact time between the membrane and the toxic metals is a crucial parameter that influences the sorption kinetics of the process [55,56]. In this instance, short contact times with the membranes can impede the system from attaining equilibrium.

Concerning the calculated selectivities (relative to Cd^{2+}), A3 membrane reached the following values for Pb^{2+}, Cr^{3+}, Cu^{2+}, Ni^{2+} and Cd^{2+} ions: 5.1, 2.5, 1.9, 1.3 and 1.0. (See Section SD5 in Supplementary Data). They follow the same order mentioned above in batch operation, though with significantly lower values, mainly for Pb^{2+} and Cr^{3+}. This result was expected in advance, taking into account the important viscous flow permeation mechanism in the membranes, which is essentially non-selective.

3.3. Interactions of toxic metals with hPAN/PVPI/GO membranes

Modifying the pristine hPAN polymer with GO and PVPI resulted in morphological and physicochemical changes in the membrane. The study of the Cd^{2+}, Cr^{3+}, Cu^{2+}, Ni^{2+}, and Pb^{2+} removal potential in multicomponent systems showed that these changes enhanced the adsorption performance of the modified membranes. The extension of the interactions between the membrane and the metal ions are affected by morphological features and physicochemical principles. Regarding the former, the rougher surface, and the asymmetric and macroporous/defects layers influence the permeation velocity distribution inside the membrane and the internal diffusion paths, which subsequently determine the adsorption kinetics. With respect to the physicochemical interactions, the increase of GO content in the modified membranes results in an increase in the oxygen content of their structure due to the functional groups, which in turn leads to an elevated number of Lewis bases in the substrate (Fig. 10). This contributes to a greater formation of coordination complexes between the modified membranes and the metal ions [50].

Despite their differences in the potential to remove metals from water, both hPAN and the modified membranes A1, A2, and A3 showed affinity for the different metal ions. Nonetheless, lower removal efficiencies and selectivities were achieved under dead-end filtration mode of operation, as the viscous flow transport and the intrinsically short membrane/adsorbate contact times made it difficult to reach equilibrium [56]. In batch, the modified membranes showed significant removal potential, mainly for Cu^{2+}, Cr^{3+}, and Pb^{2+} ions, with removal efficiencies of 50.5 %, 64.3 %, and 99.9 %, and selectivities relative to Cd^{2+} of 13.7, 24.2 and 13450, respectively, for membrane A3. The concentrations of Cu^{2+} and Pb^{2+} in the permeate meet the limit values for metal ions in waters from industrial sources and human dwellings, for the sanitary importance of drinking water, according to the World Health Organization (WHO 2022) [57] (Table 3).

Finally, membrane A3, employed in multicomponent systems, continues to demonstrate superior performance compared to most 3D materials reported in the literature, both in mono-component and

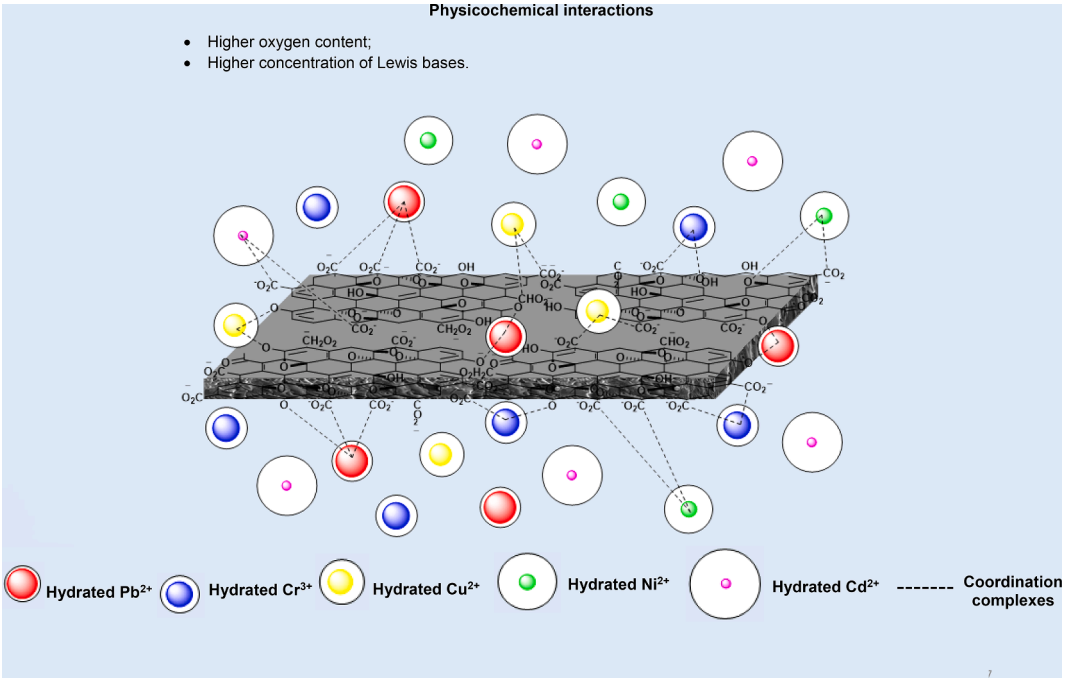

Fig. 10. Physicochemical interactions governing toxic metals adsorption onto hPAN/PVPI/GO membranes.

Table 3
Removal efficiency of A3 membrane in batch experiments together with the WHO (2022) permissible limits.

Toxic metal ions	Initial concentration (mg L^{-1})	Concentration (mg L^{-1}) after membrane treatment	Permissible limits (mg L^{-1}) of WHO (2022)
Cd(II)	1.8	1.7	0.003
Ni(II)	4.9	3.8	0.07
Cr(III)	12.2	4.3	0.05
Cu(II)	4.1	2.0	2.0
Pb(II)	10.2	0.01	0.01

multicomponent systems (Table 4). It is worth noting the favorable and significantly higher distribution coefficients ($K_i = q_i/C_i$) generally obtained for Cu^{2+}, Cr^{3+}, and Pb^{2+}, particularly the exceptionally high value for Pb^{2+}: $K = 400$ L/g *versus* the literature range of 0.000217 −0.911 L/g.

4. Economic aspects

Currently, polymeric membranes play a significant role in the treatment of wastewater and effluents, and are the primary separation medium applied in desalination processes. However, surface fouling and biofouling of these materials, low recovery, pre-treatment, and periodic cleaning are some of the shortcomings of membranes. In this scenario, there is growing interest in the development of new membranes with potential to overcome these problems and with high selectivity for target contaminants [65]. Despite the increasing interest of the academic community in the development of new membranes for removing metal ions from water, there is still a lack of economic interest in the production and full-scale application of these materials [66].

To estimate the economic aspects of new materials, two factors must be considered: the efficiency of the product and the cost associated with production. Compared to other standard membranes and composite membranes, hPAN/PVPI/GO membranes show equivalent or, in some cases, better performance in removing different metal ions from water, being highly selective for Pb^{2+}, Cr^{3+}, and Cu^{2+}. Regarding the cost associated with producing the modified membranes, considering only chemicals, the price for the A3 membrane was US$ 0.20 cm^{-2}. With the addition of transportation costs and electricity used in the process, the cost of the final membrane is around US$ 0.50 cm^{-2} [67].

Although it is possible to estimate the economic aspects associated with the production of new materials, it is difficult to assess the total costs of a credible treatment for wastewater polluted by metals. This is mainly due to the quality and quantity of the effluent volumes generated, as well as labor, passive pumping, location, and so on, parameters that influence and alter the costs of effluent treatment on a real scale. Therefore, the overall cost-benefit assessment of hPAN/PVPI/GO membranes should be examined in more detail and suggested for future use.

5. Conclusions

New hPAN membrane coated with GO layers by LbL assembly, and using PVPI as binding agent, were synthesized, characterized, and applied to the removal of metal ions from multicomponent aqueous systems. The addition of PVPI and GO to hPAN introduced oxygenated functions to the pristine polymer, increased the surface roughness of the membranes, modified the size and structure of membrane sublayers, culminating in improved efficiency to remove Cd^{2+}, Cr^{3+}, Cu^{2+}, Ni^{2+}, and Pb^{2+} ions from water.

With removal efficiencies higher than 50 % for Cu^{2+}, Cr^{3+}, and Pb^{2+}, and high equilibrium selectivities relative to Cd^{2+} (*e.g.*, 13.7, 24.2 and 13,450 for hPAN/$PVPI_3$/GO_3 membrane), two characteristics could be elucidated for the membranes: (1) The selectivity of the membranes for different metal ions suggests the formation of adsorbent-adsorbate coordination complexes promoted by the presence of Lewis bases in the substrate, and depends on properties such as the ionic radius, coordination numbers and hydration forces of the toxic metals; (2) The morphology of the modified membranes, with their higher surface roughness, asymmetric and macrovoid porous sublayers, enhanced the

Table 4
Comparison of the removal efficiency, solid concentration and distribution coefficient achieved by membrane A3 in batch experiments with other membranes from the literature.

Adsorbent	Adsorbent dosage	Metal ion	Initial concentration (mg L^{-1})	pH	Temp.	Removal efficiency (%)	Calculated solid conc. (q_i, mg g^{-1})	K_i, (L g^{-1})	Ref.
Polyamid (NDX)	–	Cu(II)	100.0	–	r.t.	29	–	–	[58]
Biochar and chitosan blend	3:7 (w/w)	Cu(II)	88.3	4.8–6.9	r.t.	57	0.12	0.0032	[59]
PEI-glycidyl polyhedral oligosilsesquioxane/GO	0.01 wt%	Cu(II)	500.0	–	r.t.	55	2750	12.2222	[53]
Comercial nanofiltration (NF270)	–	Cu(II)	2000.0	1.5	25 °C	66	–	–	[60]
TiO_2-carbon nanofibers	6 wt%	Cu(II)	300.0	7	25 °C	73	3.65	0.0451	[61]
hPAN/$PVPI_3$/GO_3	1.5 g L^{-1}	Cu(II)	4.1	5.5	25 °C	50	0.83	0.4049	This work
Poly(butylene adipate-co-terephthalate) membrane	2 % (w/w)	Cr(VI)	0.1	3	–	6	0.0003	0.0032	[62]
Poly(butylene adipate-co-terephthalate) membrane with cellulose nanostructures	2 % (w/w)	Cr(VI)	0.1	3	–	30	0.0015	0.0214	[62]
Poly(butylene adipate-co-terephthalate) membrane with modified cellulose nanostructures	2 % (w/w)	Cr(VI)	0.1	3	–	71	0.0035	0.1207	[62]
hPAN/$PVPI_3$/GO_3	1.5 g L^{-1}	Cr(III)	12.2	5.5	25 °C	64	3.14	0.7149	This work
Biochar and chitosan blend	5.5 (w/w)	Pb(II)	2.5	4.8–6.9	r.t.	54	0.00025	0.0002	[59]
PEI-glycidyl polyhedral oligosilsesquioxane/GO	1 wt%	Pb(II)	500.0	–	r.t.	78	39	0.3545	[53]
Polyphenylsulfone- COOH-GO	0.5 wt%	Pb(II)	10.0	6	r.t.	82	1.64	0.9111	[63]
TiO_2-carbon nanofibers	6 wt%	Pb(II)	300.0	7	25 °C	87	4.35	0.1115	[61]
Hyperbranched polyethyleneimine-carbon nanomaterial	1:5 (w/w)	Pb(II)	1000.0	6	25 °C	91	4.55	0.0506	[64]
hPAN/$PVPI_3$/GO_3	1.5 g L^{-1}	Pb(II)	10.2	5.5	25 °C	100	4.08	400	This work

adsorption of contaminants from water in batch and dead-end filtration operation. In addition to being highly selective for Cu^{2+}, Cr^{3+}, and Pb^{2+} in multicomponent systems, the new hPAN/PVPI/GO membranes also showed greater removal potential and distribution coefficients compared to other polymeric membranes from the literature.

CRediT authorship contribution statement

Tauany de Figueiredo Neves: Writing – review & editing, Writing – original draft, Visualization, Validation, Supervision, Software, Resources, Project administration, Methodology, Investigation, Funding acquisition, Formal analysis, Data curation, Conceptualization. **Cláudia Batista Lopes:** Writing – review & editing, Validation, Supervision, Software, Resources, Methodology, Formal analysis, Data curation. **Valmor Roberto Mastelaro:** Writing – review & editing, Software, Resources, Investigation, Formal analysis, Data curation. **Renato Falcão Dantas:** Writing – review & editing, Supervision, Resources, Project administration, Investigation, Funding acquisition. **Carlos Manuel Silva:** Writing – review & editing, Supervision, Resources, Project administration, Methodology, Investigation, Formal analysis, Data curation, Conceptualization. **Patrícia Prediger:** Writing – review & editing, Visualization, Validation, Supervision, Resources, Project administration, Methodology, Investigation, Funding acquisition, Formal analysis, Data curation, Conceptualization.

Declaration of competing interest

The authors declare that they have no known competing financial interests or personal relationships that could have appeared to influence the work reported in this paper.

Data availability

Data will be made available on request.

Acknowledgements

This work was supported by Brazilian National Research Council (CNPq, n. 311419/2022-4), Coordination for the Improvement of Higher Education Personnel (CAPES) (Finance Code 001), Fund for Support to Teaching, Research and Outreach Activities (FAEPEX, n. 2529/23 and 2207/23), Foundation of the State of São Paulo (FAPESP, n. 2013/ 07296-2, 2019/25228-0, 2022/14834-0, and 2022/11525-6), CICECO-Aveiro Institute of Materials, UIDB/50011/2020 (DOI 10.54499/UIDB/50011/2020), UIDP/50011/2020 (DOI 10.54499/UIDP/50011/2020) & LA/P/0006/2020 (DOI 10.54499/LA/P/0006/2020), National Nanotechnology Laboratory (LNNano-CNPEM, n. 20220862, 20220788 and 20230393) and Brazilian Biorenewables National Laboratory (LNBR-CNPEM, n. 20220636).

Appendix A. Supplementary data

Supplementary data to this article can be found online at https://doi.org/10.1016/j.cej.2024.155496.

References

[1] R. Proshad, M.S. Islam, T. Kormoker, A. Sayeed, S. Khadka, A.M. Idris, Potential toxic metals (PTMs) contamination in agricultural soils and foodstuffs with associated source identification and model uncertainty, Sci. Total Environ. 789 (2021) 147962, https://doi.org/10.1016/J.SCITOTENV.2021.147962.

[2] A.M. Florea, D. Büsselberg, Occurrence, use and potential toxic effects of metals and metal compounds, Biometals 2006 194. 19 (2006) 419–427. doi: 10.1007/S10534-005-4451-X.

[3] S. Rajendran, A.K. Priya, P. Senthil Kumar, T.K.A. Hoang, K. Sekar, K.Y. Chong, K. S. Khoo, H.S. Ng, P.L. Show, A critical and recent developments on adsorption technique for removal of heavy metals from wastewater-A review, Chemosphere. 303 (2022) 135146, https://doi.org/10.1016/j.chemosphere.2022.135146.

[4] M. Singh Sankhla, R. Kumar, L. Prasad, Impact of Variation in Climatic Changes in Concentration of Lead & Nickel in Yamuna River Water, Delhi, India, Mater. Today Proc. 69 (2022) 1540–1547. doi: 10.1016/j.matpr.2022.05.242.

[5] WHO, Drinking-water (World Health Organization), (2022). https://www.who.int/news-room/fact-sheets/detail/drinking-water.

[6] A. Tkaczyk, K. Mitrowska, A. Posyniak, Synthetic organic dyes as contaminants of the aquatic environment and their implications for ecosystems: A review, Sci. Total Environ. 717 (2020) 137222, https://doi.org/10.1016/j.scitotenv.2020.137222.

[7] J.R. De Andrade, M.F. Oliveira, M.G.C. Da Silva, M.G.A. Vieira, Adsorption of Pharmaceuticals from Water and Wastewater Using Nonconventional Low-Cost Materials: A Review, Ind. Eng. Chem. Res. 57 (2018) 3103–3127, https://doi.org/10.1021/acs.iecr.7b05137.

[8] A. Iqbal, E. Cevik, A. Mustafa, T.F. Qahtan, M. Zeeshan, A. Bozkurt, Emerging developments in polymeric nanocomposite membrane-based filtration for water purification: A concise overview of toxic metal removal, Chem. Eng. J. 481 (2024) 148760, https://doi.org/10.1016/j.cej.2024.148760.

[9] Y. He, C. Yi, X. Zhang, W. Zhao, D. Yu, Magnetic graphene oxide: Synthesis approaches, physicochemical characteristics, and biomedical applications, TrAC Trends Anal. Chem. 136 (2021) 116191, https://doi.org/10.1016/J.TRAC.2021.116191.

[10] S.P. Sundaran, C.R. Reshmi, P. Sagitha, O. Manaf, A. Sujith, Multifunctional graphene oxide loaded nanofibrous membrane for removal of dyes and coliform from water, J. Environ. Manage. 240 (2019) 494–503, https://doi.org/10.1016/j.jenvman.2019.03.105.

[11] Y. Li, Y. Wang, Z. Liu, L. Jiang, H. Yang, Z. Xu, Separation of anionic dye mixtures b y Al-metal-organic framework filled polyacrylonitrile-ethanolamine membrane and its modified product, J. Clean. Prod. 284 (2021) 124778, https://doi.org/10.1016/J.JCLEPRO.2020.124778.

[12] D.I. Petukhov, O.O. Kapitanova, E.A. Eremina, E.A. Goodilin, Preparation, chemical features, structure and applications of membrane materials based on graphene oxide, Mendeleev Commun. 31 (2021) 137–148, https://doi.org/10.1016/J.MENCOM.2021.03.001.

[13] E.F. Diogo Januário, N. de Camargo Lima Beluci, T.B. Vidovix, M.F. Vieira, R. Bergamasco, A.M. Salcedo Vieira, Functionalization of membrane surface by layer-by-layer self-assembly method for dyes removal, Process Saf. Environ. Prot. 134 (2020) 140–148. doi: 10.1016/J.PSEP.2019.11.030.

[14] M. Patel, R. Patel, W.S. Chi, J.H. Kim, J.S. Sung, Antibacterial behaviour of quaternized poly(vinyl chloride)-g-poly(4-vinyl pyridine) graft copolymers, Chinese, J. Polym. Sci. 33 (2015) 265–274, https://doi.org/10.1007/s10118-015-1577-3.

[15] J.A. Moleon, A. Ontiveros-Ortega, E. Gimenez-Martin, I. Plaza, Effect of N-cetylpyridinium chloride in adsorption of graphene oxide onto polyester, Dye. Pigment. 122 (2015) 310–316, https://doi.org/10.1016/j.dyepig.2015.07.004.

[16] T.F. Neves, N. Barticiotto Dalarme, P.M.M. da Silva, R. Landers, C. Siqueira Franco Picone, P. Prediger, Novel magnetic chitosan/quaternary ammonium salt graphene oxide composite applied to dye removal, J. Environ. Chem. Eng. 8 (2020) 103820. doi: 10.1016/j.jece.2020.103820.

[17] W.S. Hummers, R.E. Offeman, Preparation of Graphitic Oxide, J. Am. Chem. Soc. 80 (1958) 1339, https://doi.org/10.1021/ja01539a017.

[18] T. de F. Neves, N.G. Camparotto, E.A. Rodrigues, V.R. Mastelaro, R.F. Dantas, P. Prediger, New graphene oxide-safranin modified@polyacrylonitrile membranes for removal of emerging contaminants: The role of chemical and morphological features, Chem. Eng. J. 446 (2022) 137176. doi: 10.1016/J.CEJ.2022.137176.

[19] M. Hu, B. Mi, Layer-by-layer assembly of graphene oxide membranes via electrostatic interaction, J. Memb. Sci. 469 (2014) 80–87, https://doi.org/10.1016/j.memsci.2014.06.036.

[20] N. Bicak, M. Gazi, Quantitative quaternization of poly(4-vinyl pyridine), J. Macromol. Sci. - Pure Appl. Chem. 40 (2003) 585–591, https://doi.org/10.1081/MA-120020865.

[21] E. Halakoo, X. Feng, Layer-by-layer assembled membranes from graphene oxide and polyethyleneimine for ethanol and isopropanol dehydration, Chem. Eng. Sci. 216 (2020) 115488, https://doi.org/10.1016/j.ces.2020.115488.

[22] P. Sharma, S. Tripathi, D. Purchase, R. Chandra, Integrating phytoremediation into treatment of pulp and paper industry wastewater : Field observations of native plants for the detoxification of metals and their potential as part of a multidisciplinary strategy, J. Environ. Chem. Eng. 9 (2021) 105547, https://doi.org/10.1016/j.jece.2021.105547.

[23] P. Sharma, H.M.N. Iqbal, R. Chandra, Case Studies in Chemical and Environmental Engineering Evaluation of pollution parameters and toxic elements in wastewater of pulp and paper industries in India : A case study, Case Stud. Chem. Environ. Eng. 5 (2022) 100163, https://doi.org/10.1016/j.cscee.2021.100163.

[24] K. Curo, J. Valverde Flores, Removal of Lead wastewater from the thermal stabilizer industry by chemical precipitation, J Energy Environ. Sci. 1 (2017) 17, https://doi.org/10.32829/eesj.v1i1.27.

[25] T. de Figueiredo Neves, P. Kushima Assano, L. Rodrigues Sabino, W. Bardelin Nunes, P. Prediger, Influence of Adsorbent/Adsorbate Interactions on the Removal of Cationic Surfactants from Water by Graphene Oxide, Water, Air. Soil Pollut. 231 (2020) 1–22, https://doi.org/10.1007/s11270-020-04669-w.

[26] P. Chen, H. Li, S. Song, X. Weng, D. He, Y. Zhao, Adsorption of dodecylamine hydrochloride on graphene oxide in water, Results Phys. 7 (2017) 2281–2288, https://doi.org/10.1016/j.rinp.2017.06.054.

[27] P. Prediger, T. Cheminski, T. de Figueiredo Neves, W.B. Nunes, L. Sabino, C.S. F. Picone, R.L. Oliveira, C.R.D. Correia, Graphene oxide nanomaterials for the removal of non-ionic surfactant from water, J. Environ Chem. Eng. 6 (2018), https://doi.org/10.1016/j.jece.2018.01.072.

[28] M.A. Chinelatto, J.A.M. Agnelli, S.V. Canevarolo, Synthesis and characterization of copolymers from hindered amines and vinyl monomers, Polimeros. 24 (2014) 30–36, https://doi.org/10.4322/polimeros.2014.046.
[29] J. Fang, Y. Xuan, Q. Li, Preparation of polystyrene spheres in different particle sizes and assembly of the PS colloidal crystals, Sci. China Technol. Sci. 53 (2010) 3088–3093, https://doi.org/10.1007/s11431-010-4110-5.
[30] Y. Chen, W. Zhao, J. Zhang, Preparation of 4-vinylpyridine (4VP) resin and its adsorption performance for heavy metal ions, RSC Adv. 7 (2017) 4226–4236, https://doi.org/10.1039/c6ra26813g.
[31] N.G. Khaligh, Investigation of the catalytic activity of poly(4-vinylpyridine) supported iodine as a new, efficient and recoverable catalyst for regioselective ring opening of epoxides, RSC Adv. 2 (2012) 3321–3327, https://doi.org/10.1039/c2ra20080e.
[32] H. Zhang, L. Quan, A. Gao, Y. Tong, F. Shi, L. Xu, The structure and properties of polyacrylonitrile nascent composite fibers with grafted multi walled carbon nanotubes prepared by wet spinning method, Polymers (basel). 11 (2019) 422, https://doi.org/10.3390/POLYM11030422.
[33] X.-G. Dong, C.-G. Wang, J. Chen, W.-W. Cao, Crystallinity development in polyacrylonitrile nascent fibers during coagulation, J. Polym. Res. 15 (2008) 125–130, https://doi.org/10.1007/s10965-007-9151-5.
[34] D.A. Skoog, F.J. Holler, S.R. Crouch, Principles of instrumental analysis, 7[a], 2007. doi: 10.1017/CBO9781107415324.004.
[35] W.S. Hung, Q.F. An, M. De Guzman, H.Y. Lin, S.H. Huang, W.R. Liu, C.C. Hu, K. R. Lee, J.Y. Lai, Pressure-assisted self-assembly technique for fabricating composite membranes consisting of highly ordered selective laminate layers of amphiphilic graphene oxide, Carbon n. y. 68 (2014) 670–677, https://doi.org/10.1016/j.carbon.2013.11.048.
[36] H. Guo, Y. Ma, P. Sun, S. Cui, Z. Qin, Y. Liang, Self-cleaning and antifouling nanofiltration membranes—superhydrophilic multilayered polyelectrolyte/CSH composite films towards rejection of dyes, RSC Adv. 5 (2015) 63429–63438, https://doi.org/10.1039/C5RA11438A.
[37] S. Yang, H. Zhen, B. Su, Polyimide thin film composite (TFC) membranes via interfacial polymerization on hydrolyzed polyacrylonitrile support for solvent resistant nanofiltration, RSC Adv. 7 (2017) 42800–42810, https://doi.org/10.1039/C7RA08133B.
[38] J. Jauhari, M.R. Almafie, L. Marlina, Z. Nawawi, I. Sriyanti, Physicochemical properties and performance of graphene oxide/polyacrylonitrile composite fibers as supercapacitor electrode materials, RSC Adv. 11 (2021) 11233–11243, https://doi.org/10.1039/D0RA10257A.
[39] M. Dutta, S. Bhattacharjee, S. De, Separation of reactive dyes from textile effluent by hydrolyzed polyacrylonitrile hollow fiber ultrafiltration quantifying the transport of multicomponent species through charged membrane pores, Sep. Purif. Technol. 234 (2020) 116063, https://doi.org/10.1016/J.SEPPUR.2019.116063.
[40] L. Pérez-Álvarez, L. Ruiz-Rubio, I. Moreno, J.L. Vilas-Vilela, Characterization and optimization of the alkaline hydrolysis of polyacrylonitrile membranes, Polymers (basel). 11 (2019) 1–11, https://doi.org/10.3390/polym11111843.
[41] B. Gieroba, A. Sroka-Bartnicka, P. Kazimierczak, G. Kalisz, A. Lewalska-Graczyk, V. Vivcharenko, R. Nowakowski, I.S. Pieta, A. Przekora, Spectroscopic studies on the temperature-dependent molecular arrangements in hybrid chitosan/1,3-β-D-glucan polymeric matrices, Int. J. Biol. Macromol. 159 (2020) 911–921, https://doi.org/10.1016/j.ijbiomac.2020.05.155.
[42] N. de C.L. Beluci, G.A.P. Mateus, C.S. Miyashiro, N.C. Homem, R.G. Gomes, M.R. Fagundes-Klen, R. Bergamasco, A.M.S. Vieira, Hybrid treatment of coagulation/flocculation process followed by ultrafiltration in TIO 2 -modified membranes to improve the removal of reactive black 5 dye, Sci. Total Environ. 664 (2019) 222–229. doi: 10.1016/j.scitotenv.2019.01.199.
[43] E.F.D. Januário, T.B. Vidovix, N. de C.L. Beluci, R.M. Paixão, L.H.B.R. da Silva, N. C. Homem, R. Bergamasco, A.M.S. Vieira, Advanced graphene oxide-based membranes as a potential alternative for dyes removal: A review, Sci. Total Environ. 789 (2021) 147957. doi: 10.1016/J.SCITOTENV.2021.147957.
[44] M.F. Twibi, M.H.D. Othman, S.K. Hubadillah, S.A. Alftessi, M.R. Bin Adam, A.F. Ismail, M.A. Rahman, J. Jaafar, Y.O. Raji, M.H. Abd Aziz, M.N.B.M. Sokri, H. Abdullah, R. Naim, Hydrophobic mullite ceramic hollow fibre membrane (Hy-MHFM) for seawater desalination via direct contact membrane distillation (DCMD), J. Eur. Ceram. Soc. 41 (2021) 6578–6585. doi: 10.1016/J.JEURCERAMSOC.2021.06.024.
[45] T. Ahmad, C. Guria, A. Mandal, Optimal synthesis of high fouling-resistant PVC-based ultrafiltration membranes with tunable surface pore size distribution and ultralow water contact angle for the treatment of oily wastewater, Sep. Purif. Technol. 257 (2021) 117829, https://doi.org/10.1016/J.SEPPUR.2020.117829.
[46] V.R.S.S. Mokkapati, D.Y. Koseoglu-Imer, N. Yilmaz-Deveci, I. Mijakovic, I. Koyuncu, Membrane properties and anti-bacterial/anti-biofouling activity of polysulfone-graphene oxide composite membranes phase inversed in graphene oxide non-solvent, RSC Adv. 7 (2017) 4378–4386, https://doi.org/10.1039/C6RA25015G.
[47] Z. Qiu, X. Ji, C. He, Fabrication of a loose nanofiltration candidate from Polyacrylonitrile/Graphene oxide hybrid membrane via thermally induced phase separation, J. Hazard. Mater. 360 (2018) 122–131, https://doi.org/10.1016/J.JHAZMAT.2018.08.004.
[48] N. de C.L. Beluci, N.C. Homem, M.T.S.P. Amorim, R. Bergamasco, A.M.S. Vieira, Biopolymer extracted from Moringa oleifera Lam. in conjunction with graphene oxide to modify membrane surfaces, Environ. Technol. (United Kingdom). 41 (2020) 3069–3080. doi: 10.1080/09593330.2019.1597172.
[49] H.F.M. Austria, R.L.G. Lecaros, W.S. Hung, L.L. Tayo, C.C. Hu, H.A. Tsai, K.R. Lee, J.Y. Lai, Investigation of salt penetration mechanism in hydrolyzed polyacrylonitrile asymmetric membranes for pervaporation desalination, Desalination. 463 (2019) 32–39, https://doi.org/10.1016/J.DESAL.2019.04.012.
[50] T.A. Saleh, I. Ali, Synthesis of polyamide grafted carbon microspheres for removal of rhodamine B dye and heavy metals, J. Environ. Chem. Eng. 6 (2018) 5361–5368, https://doi.org/10.1016/j.jece.2018.08.033.
[51] D. Upreti, A. Rajendran, N. Lenka, R. Srivastava, R. Sen Gupta, B. Maiti, S. Bose, T. U. Patro, Designing a robust biocompatible porous polymeric membrane using Laponite and graphene oxide for versatile and selective adsorption of water contaminants, Chem. Eng. J. 464 (2023) 142738. doi: 10.1016/j.cej.2023.142738.
[52] F. Zareei, S.M. Hosseini, A new type of polyethersulfone based composite nanofiltration membrane decorated by cobalt ferrite-copper oxide nanoparticles with enhanced performance and antifouling property, Sep. Purif. Technol. 226 (2019) 48–58, https://doi.org/10.1016/j.seppur.2019.05.077.
[53] S. Bandehali, A. Moghadassi, F. Parvizian, Y. Zhang, S.M. Hosseini, J. Shen, New mixed matrix PEI nanofiltration membrane decorated by glycidyl-POSS functionalized graphene oxide nanoplates with enhanced separation and antifouling behaviour: Heavy metal ions removal, Sep. Purif. Technol. 242 (2020) 116745, https://doi.org/10.1016/j.seppur.2020.116745.
[54] B. Tansel, J. Sager, T. Rector, J. Garland, R.F. Strayer, L. Levine, M. Roberts, M. Hummerick, J. Bauer, Significance of hydrated radius and hydration shells on ionic permeability during nanofiltration in dead end and cross flow modes, Sep. Purif. Technol. 51 (2006) 40–47, https://doi.org/10.1016/j.seppur.2005.12.020.
[55] T.R. Sahoo, B. Prelot, Adsorption processes for the removal of contaminants from wastewater: the perspective role of nanomaterials and nanotechnology, Nanomater. Detect. Remov. Wastewater Pollut. (2020) 161–222. doi: 10.1016/B978-0-12-818489-9.00007-4.
[56] H.K. Agbovi, L.D. Wilson, 1 - Adsorption processes in biopolymer systems: fundamentals to practical applications, in: S. Kalia (Ed.), Nat. Polym. Green Adsorbents Water Treat., 1[a], INC, 2021: pp. 1–51. doi: 10.1016/b978-0-12-820541-9.00011-9.
[57] World Health Organization, Guidelines for drinking-water quality: fourth edition incorporating the first and second addenda, 2022.
[58] W.N.A.S. Abdullah, S. Tiandee, W. Lau, F. Aziz, A.F. Ismail, Potential use of nanofiltration like-forward osmosis membranes for copper ion removal, Chinese, J Chem. Eng. 28 (2020) 420–428, https://doi.org/10.1016/j.cjche.2019.05.016.
[59] A. Hussain, J. Maitra, K.A. Khan, Development of biochar and chitosan blend for heavy metals uptake from synthetic and industrial wastewater, Appl. Water Sci. 7 (2017) 4525–4537, https://doi.org/10.1007/s13201-017-0604-7.
[60] B.A.M. Al-Rashdi, D.J. Johnson, N. Hilal, Removal of heavy metal ions by nanofiltration, Desalination. 315 (2013) 2–17, https://doi.org/10.1016/j.desal.2012.05.022.
[61] P.S. Kumar, K. Venkatesh, E.L. Gui, S. Jayaraman, G. Singh, G. Arthanareeswaran, Electrospun carbon nanofibers/TiO2-PAN hybrid membranes for effective removal of metal ions and cationic dye, Environ. Nanotechnology, Monit. Manag. 10 (2018) 366–376. doi: 10.1016/j.enmm.2018.08.006.
[62] R.F.S. Barbosa, A.G. Souza, H.F. Maltez, D.S. Rosa, Chromium removal from contaminated wastewaters using biodegradable membranes containing cellulose nanostructures, Chem. Eng. J. 395 (2020) 125055, https://doi.org/10.1016/j.cej.2020.125055.
[63] A.K. Shukla, J. Alam, M. Alhoshan, L. Arockiasamy Dass, F.A.A. Ali, M.R. Muthumareeswaran, U. Mishra, M.A. Ansari, Removal of heavy metal ions using a carboxylated graphene oxide-incorporated polyphenylsulfone nanofiltration membrane, Environ. Sci. Water Res. Technol. 4 (2018) 438–448. doi: 10.1039/c7ew00506g.
[64] M.A. Tofighy, T. Mohammadi, Divalent heavy metal ions removal from contaminated water using positively charged membrane prepared from a new carbon nanomaterial and HPEI, Chem. Eng. J. 388 (2020) 124192, https://doi.org/10.1016/j.cej.2020.124192.
[65] N.A.A. Qasem, R.H. Mohammed, D.U. Lawal, Removal of heavy metal ions from wastewater: a comprehensive and critical review, Npj Clean Water. 4 (2021) 36, https://doi.org/10.1038/s41545-021-00127-0.
[66] N.G. Camparotto, T. de Figueiredo Neves, J. de Souza Vendemiatti, B.T. dos Santos, M.G.A. Vieira, P. Prediger, Adsorption of contaminants by nanomaterials synthesized by green and conventional routes: a critical review, Environ. Sci. Pollut. Res. 31 (2024) 12683–12721. doi: 10.1007/s11356-024-31922-0.
[67] S.K. Srivastava, V.K. Gupta, I.S. Yadav, D. Mohan, Removal of 2,4-dinitrophenol using bagasse fly ash - a sugar industry waste material, Fresenius Environ. Bull. 4 (1995) 550–557.